

A Flexible Fiber-Based Supercapacitor–Triboelectric-Nanogenerator Power System for Wearable Electronics

Jie Wang, Xiuhan Li, Yunlong Zi, Sihong Wang, Zhaoling Li, Li Zheng, Fang Yi, Shengming Li, and Zhong Lin Wang*

The development of renewable and sustainable energy is the most important issue due to the tremendous energy consumption of modern society. Some green energy sources such as solar and wind power are both intermittent, since the sun does not shine during the night and wind does not blow on demand.^[1] Other energy harvesting techniques such as nanogenerators can easily and efficiently convert mechanical energy in the living/working environment into electric energy, but they usually have uncontrollable fluctuation/instability in their outputs that are greatly influenced by changes in the ambient environment.^[2,3] For example, although the recently invented triboelectric nanogenerator (TENG) is a powerful technique with low-cost, high efficiency, and environmental friendly features,^[4–11] the output electric power are pulses with irregular magnitude depending on the strength of the mechanical triggering. Therefore, it cannot be directly used to drive most electronic devices that require a stable and continuous input power.^[12] Therefore, it is essential to adopt electrical energy storage systems for providing a stable and durable output. Among them, lithium-ion batteries and supercapacitors are the state-of-the-art. Supercapacitors, also called electrochemical capacitors, are superior to lithium-ion batteries in power density, life cycles, environmental benignancy, etc.^[13–17] Hence, given the nature of the pulse energy generated by a TENG at low frequency, supercapacitors may be a better choice.

On the other hand, owing to the rapid growth of portable and wearable consumer electronics, such as wearable displays, on-body sensors, artificial electronic skin, and distributed sensors,^[18] enormous effort has been devoted to flexible, weavable, and integratable electronics to meet the demands of modern

society. The development of wearable electronics has inspired much work in designing flexible and wearable fiber supercapacitors (FSCs) as a power provider. Since Wang's group reported the first prototype of fiber supercapacitors made from ZnO nanowires and/or coated by MnO₂,^[19] FSCs prepared from various electrode materials and structures have been widely explored. Peng and co-workers designed FSCs by twisting two aligned multiwall carbon nanotube (MWCNT) fibers^[20] and by coaxial structure of titania-nanotube-modified Ti wire and aligned MWCNT sheets.^[21] Qu and co-workers prepared all-in-one single-fiber supercapacitors through region-specific reduction of graphene oxide.^[22] Chou and co-workers fabricated a carbon-nanotube-fiber-based supercapacitor.^[23] Shen and co-workers synthesized Mn₂O₃ cube arrays/carbon wire electrodes for FSCs and optimized their performance by tuning the device architectures.^[24] However, the reported FSCs have had low specific capacitance, such as 1.2 mF cm⁻² in ref. [22] and 4.28 mF cm⁻² (corresponding volumetric capacitance of 11.40 F cm⁻³) in ref. [23].

In this work, a flexible and weavable self-charging power system consisting of FSCs and a fiber-based TENG (FTENG) is reported for the first time, which is also the first prototype for wearable electronics that can harvest mechanical energy from human motion. We first synthesized RuO₂·xH₂O on the surface of carbon fiber (RuO₂·xH₂O@CF) to serve as the electrodes of FSC with a diameter of ≈70 μm. By using a vapor-phase hydrothermal method, we managed to obtain high conductivity of both ion and electron simultaneously in the RuO₂·xH₂O. As a result, the FSC is significantly optimized with a remarkable specific capacitance of 83.5 F cm⁻³ (3.2 mF cm⁻¹ and 146 mF cm⁻²). Second, a new kind of FTENG was designed via poly(dimethylsiloxane) (PDMS) coated on carbon wire electrodes. Third, this novel FSC and FTENG were integrated into an effective self-charging power system.

As illustrated in Figure 1a, three FSCs and an FTENG were integrated via a rectifier to form the fiber-based supercapacitor–triboelectric nanogenerator power system. The FSC was symmetrically assembled from two RuO₂·xH₂O@CF electrodes. RuO₂·xH₂O was synthesized on carbon fiber bundles by using a vapor-phase hydrothermal method to form the binder-free fiber electrodes (Figure S1a, Supporting Information), and its details can be found in the Experimental Section and the Supporting Information. Figure 1b shows a low-magnification scanning electron microscopy (SEM) image of the as-synthesized RuO₂·xH₂O@carbon fibers, which clearly shows that several carbon fibers were assembled to a bundle with a diameter of ≈70 μm. The higher-magnification SEM image shown

Dr. J. Wang, Dr. X. Li, Dr. Y. Zi, Dr. S. Wang, Z. Li,
Dr. L. Zheng, F. Yi, S. Li, Prof. Z. L. Wang
School of Materials Science and Engineering
Georgia Institute of Technology
Atlanta, GA 30332, USA
E-mail: zhong.wang@mse.gatech.edu



Dr. J. Wang
Electronic Materials Research Laboratory
Key Laboratory of the Ministry of Education & International Center of
Dielectric Research
Xi'an Jiaotong University
Xi'an 710049, China
Prof. Z. L. Wang
Beijing Institute of Nanoenergy and Nanosystems
Chinese Academy of Sciences
Beijing 100083, China

DOI: 10.1002/adma.201501934

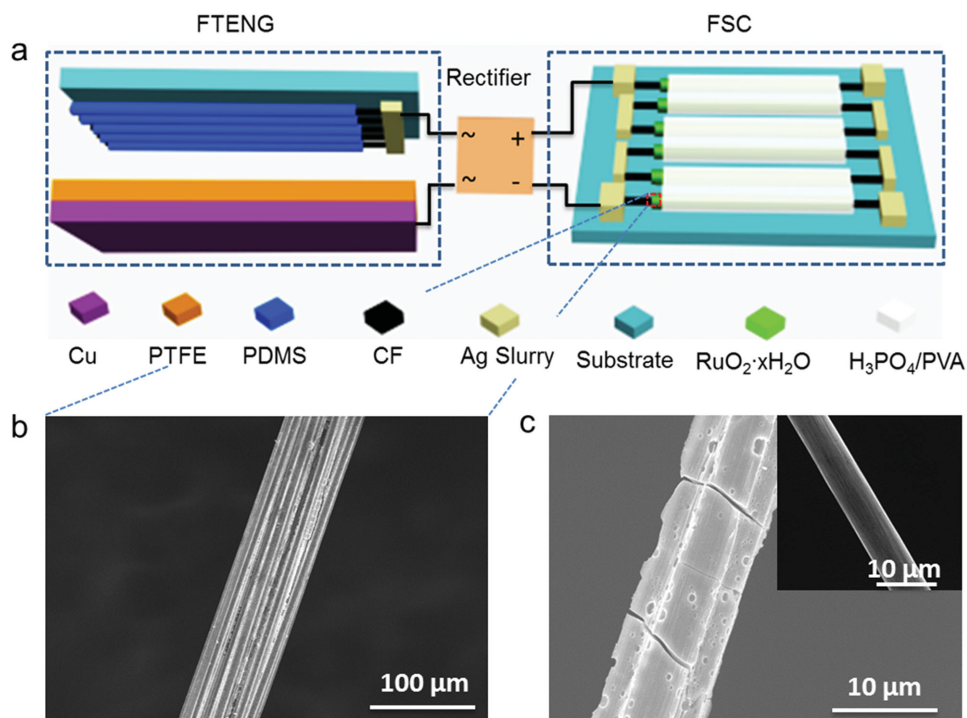


Figure 1. a) Schedule of integrating the fiber-based supercapacitor–triboelectric nanogenerator power system. b) SEM image of $\text{RuO}_2 \cdot x\text{H}_2\text{O}$ @CF electrode of FSC. c) $\text{RuO}_2 \cdot x\text{H}_2\text{O}$ coating on a single fiber, with a single carbon fiber shown in the up-right corner.

in Figure 1c reveals that $\text{RuO}_2 \cdot x\text{H}_2\text{O}$ coated on a single carbon fiber presents the typical “cracked mud” morphology.^[25] As a contrast, a single bare fiber exhibits a smooth surface, shown in the upper-right corner of Figure 1c. To uncover the composition of the as-synthesized product, energy dispersive spectroscopy (EDS) analysis was carried out on a random selected area of the fiber electrodes. The EDS spectrum (Figure S2a, Supporting Information) revealed that the as-synthesized sample is $\text{RuO}_2 \cdot 0.4\text{H}_2\text{O}$. It is very close to the ideal structure, $\text{RuO}_2 \cdot 0.5\text{H}_2\text{O}$, which can reach the most effective balance between electron transport and proton transport, both of which are essential for energy storage, because the charging/discharging process needs both transports simultaneously in the active material.^[26] But in order to compensate the low conductivity of carbon fibers, RuO_2 here was designed to have less water to achieve higher electron conductivity. The crystallographic structure of $\text{RuO}_2 \cdot 0.4\text{H}_2\text{O}$ was further analyzed by X-ray diffraction (XRD) (Figure S2b, Supporting Information). The results reveal that as-synthesized $\text{RuO}_2 \cdot 0.4\text{H}_2\text{O}$ was typical amorphous with partly rutile crystalline structure, which is an essential factor to simultaneously obtain high ion and electron conductivity, because electron conduction is supported by the rutile-like nanocrystals and proton conduction is facilitated by the structural water, as shown in refs. [27] and [28].

The electrochemical capacitance properties of the $\text{RuO}_2 \cdot 0.4\text{H}_2\text{O}$ @CF were further examined by electrochemical impedance spectra (EIS), cyclic voltammetry (CV) and galvanostatic charging/discharging (GCD) techniques in a conventional three-electrode system in 1 M H_3PO_4 solution. The $\text{RuO}_2 \cdot 0.4\text{H}_2\text{O}$ @CF electrode was used as the working

electrode, a Pt wire served as the counter electrode, and a saturated calomel electrode (SCE) as the reference electrode. The EIS result (Figure 2a) indicates that the $\text{RuO}_2 \cdot 0.4\text{H}_2\text{O}$ @CF electrode has almost ideal electrochemical capacitance behavior, i.e., the imaginary part of the impedance at low frequency region being perpendicular to the real part.^[29] The capacitance (C), calculated by Equation (1) as a function of frequency (f), is shown in the up-right corner of Figure 2a.

$$C = -1 / (2\pi f Z_{\text{im}}) \quad (1)$$

In Equation (1), Z_{im} is the imaginary part of the impedance. The capacitance of $\text{RuO}_2 \cdot 0.4\text{H}_2\text{O}$ @CF electrode was up to 3.1 mF at 0.01 Hz while that of the pure carbon fiber electrode was only $\approx 19 \mu\text{F}$ (Figure S3, Supporting Information), representing that the contribution of the carbon fibers is negligible. Moreover, there is a capacitance plateau between 0.01 and 1 Hz, indicating a fast charging/discharging process. On its CV curves (Figure 2b), there is a broad peak at the potential of ≈ 0.4 V versus SCE, which is a sign of pseudocapacitance. In addition, no obvious current decay was observed during reversing the potential sweep, even at a scanning rate of 40 mV s^{-1} , indicating a fast kinetic process. The triangle-shaped galvanostatic charging/discharging curves (Figure 2c) are typical for supercapacitors. There is no obvious ohm-drop (IR -Drop) phenomenon found, even at a short discharging time of 20 s, which confirms the perfect capacitance behavior again. The specific capacitance can be calculated from GCD curves by the following equation:

$$C = I \times t / V \quad (2)$$

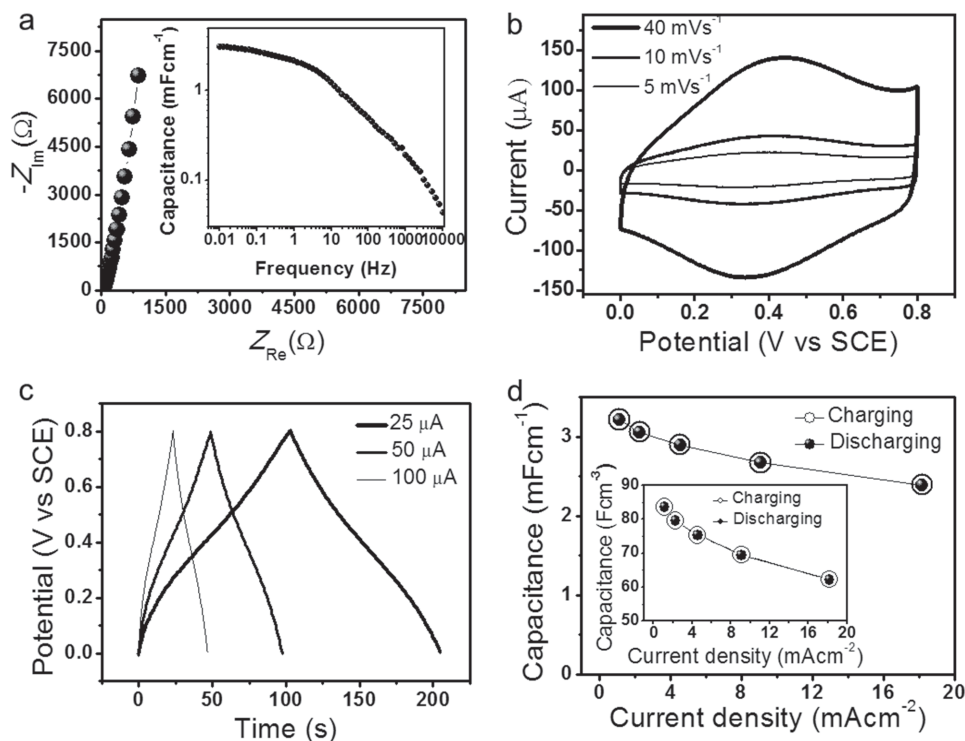


Figure 2. Capacitance properties of $\text{RuO}_2 \cdot x\text{H}_2\text{O}@\text{CF}$ electrodes in 1 M H_3PO_4 solution. a) Electrochemical impedance spectroscopy, with an inset plot of capacitance versus frequency, b) CV curves at various scanning rates, c) GCD curves at different current density, and d) charging/discharging specific capacitance as a function of current density, inset shows the volume specific capacitance.

where I denotes the discharging current, t is charging/discharging time, and V represents voltage window. Since the mass specific capacitance (F g^{-1}) is not suitable for fiber-based supercapacitors, the volume specific capacitance (F cm^{-3}) as well as the area and length specific capacitance (F cm^{-2} and F cm^{-1}) were calculated to be up to 83.5 F cm^{-3} , 146 F cm^{-2} , and 3.2 F cm^{-1} at a current density of 1.14 mA cm^{-2} (Figure 2d). Furthermore, its energy density was up to 26.7 J cm^{-3} . Here, the diameter of the electrode was determined by SEM shown in Figure 1b, since they came from the same $\text{RuO}_2 \cdot 0.4\text{H}_2\text{O}@\text{CF}$ bundle. To our knowledge, this volume specific capacitance is the highest so far for thread-like supercapacitors,^[19–23,30] which can be attributed to both the high specific capacitance of $\text{RuO}_2 \cdot x\text{H}_2\text{O}$ prepared by the vapor-phase hydrothermal method and the small electrode diameter enlarging the active material ratio. It should be noted that the capacitance calculated from EIS is slightly smaller than the value from GCD data, which can be explained by the redox switch hysteresis of metal oxide.^[31] More importantly, the specific capacitance can still be maintained at a fairly high level (62.2 F cm^{-3} , 107 F cm^{-2} , and 2.35 F cm^{-1}) even at a high current density of 18.2 mA cm^{-2} , and its power density is up to 4.12 W cm^{-3} , both of which manifest the fast charging/discharging ability and high power density. Moreover, the Coulombic efficiency (discharging capacitance/charging capacitance) is nearly 100%. Therefore, $\text{RuO}_2 \cdot 0.4\text{H}_2\text{O}@\text{CF}$ can be recognized as a high-performance supercapacitor electrode.

Our flexible solid-state FSCs were made of two identical $\text{RuO}_2 \cdot 0.4\text{H}_2\text{O}@\text{CF}$ electrodes and $\text{H}_3\text{PO}_4/\text{PVA}$ gel electrolyte, where a polytetrafluoroethylene (PTFE) film acted as the

flexible substrate (Figure 3a). The electrodes were assembled in parallel pattern with a space of 1 mm to reduce the leakage current of supercapacitor. The electrochemical capacitance properties of the planar FSC and the multi-time bent FSC (Figure 3b) were tested by the CV method at a scanning rate of 2 mV s^{-1} . The bent radius and diameter are 2 mm and $70 \mu\text{m}$, respectively. So the calculated strain is 1.72%.^[32] Both of them exhibit the typical and almost overlapping rectangle-like CV curves (Figure 3c), indicating them to be excellent supercapacitors. The 100-time bent one retains 94% capacitance, which enables an FSC of great flexibility. Its flexibility was further confirmed by GCD results at a current load of 0.5 mA cm^{-2} (Figure 3d). The classical triangle-shaped charging/discharging curves and an almost identical capacitance were found in both results. The initial capacitance was calculated to be 1.76 mF and the Coulombic efficiency is 96.4%. After bending 100 times, the capacitance remains as 1.66 mF and the Coulombic efficiency is 96.2%. As further demonstrated in Figure 3e, two $\text{RuO}_2 \cdot 0.4\text{H}_2\text{O}@\text{CF}$ electrodes were twisted to form a supercapacitor (marked area), which was weaved together with $\text{RuO}_2 \cdot 0.4\text{H}_2\text{O}@\text{CF}$ electrodes into flexible textiles. Besides the flexibility of carbon fiber itself, the remarkable flexibility of the FSC is attributed to the “cracked mud” structure of $\text{RuO}_2 \cdot 0.4\text{H}_2\text{O}$ (Figure 1c) accommodating the mechanical stress. For another critical parameter to supercapacitors, i.e., cycling stability, although the capacitance had some subtle fluctuation during the cycling test, it was able to maintain as much as 94% after 5000 continual cycles at a current density of 4 mA cm^{-2} (Figure 3f). Similar EIS spectra were found before

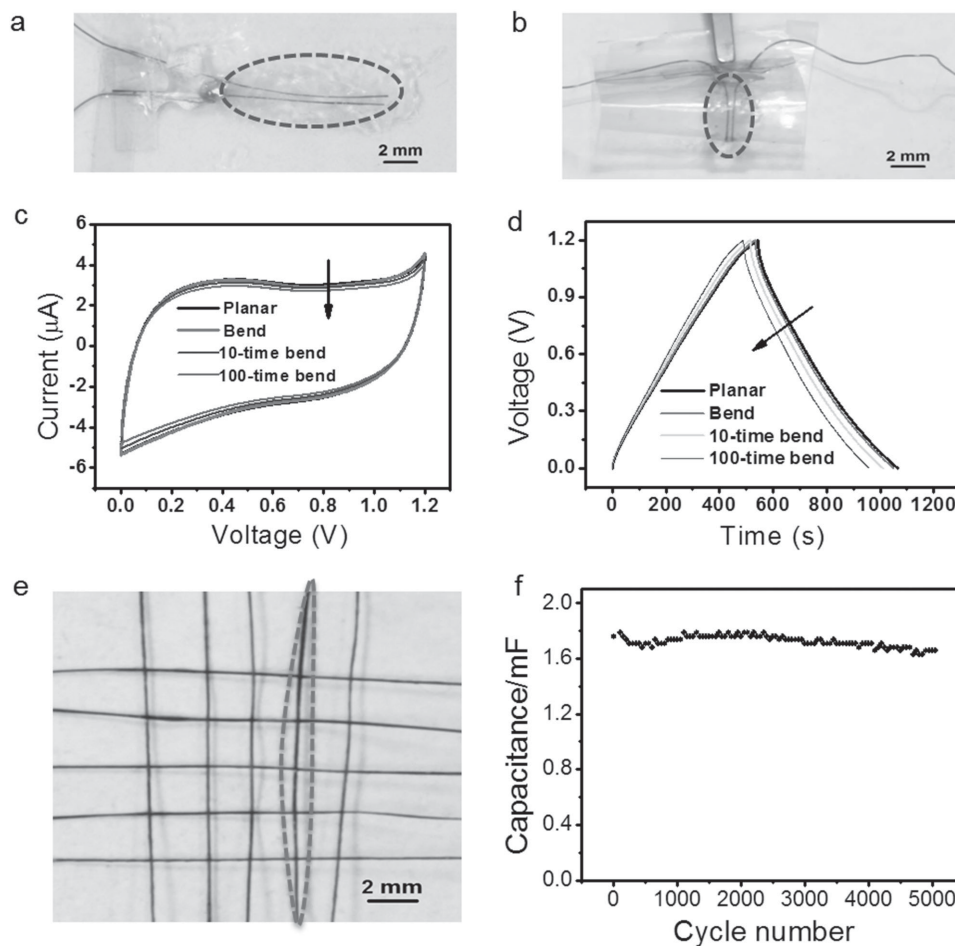


Figure 3. Performance of the solid-state FSC with $\text{H}_3\text{PO}_4/\text{PVA}$ gel electrolyte. a) Planar FSC, b) bent FSC, c) CV curves of the planar and bent FSC, d) GCD curves of two FSCs, e) twisted FSC (marked area) and $\text{RuO}_2 \cdot 0.4\text{H}_2\text{O}@\text{CF}$ electrodes woven into a textile structure with each other, and f) cycling performance of the flexible FSC at the current density of 2.5 mA cm^{-2} .

and after 5000 cycles (Figure S4, Supporting Information). Both results indicate a notable cycling performance.

In order to extend the output voltage of our flexible FSC, three of them were connected in series by silver paste on an acrylic substrate. The three-series FSC exhibited excellent electrochemical performance, revealed by EIS and the GCD method, as shown in Figure S5 (Supporting Information). It was charged to 2.5 V even at a fairly low current of $0.5 \mu\text{A}$ with a Coulombic efficiency of 94%, which suggests a very low leakage current and hence enables its great effectiveness as an energy-storage utility.

The structure of FTENG is shown in Figure 1a. PDMS/carbon wire electrodes were designed for our new fiber-based TENG so that they can easily be bent to a desired shape. PDMS coated on carbon fibers was used as the triboelectric layer and the carbon fibers as the collecting electrode. The length of the carbon fiber was 7 cm and that of PDMS was 5 cm. The uncoated terminal part of the carbon fiber was used to connect to the outer electrode. Nine carbon fibers coated by PDMS were adhered in parallel to the supporting acrylic substrate, with a diameter of 0.25 cm and a length of 5 cm. PTFE was employed as another triboelectric layer and coated with copper as the con-

ducting film. It was tailored into a $7 \text{ cm} \times 5 \text{ cm}$ rectangle, and then adhered on the acrylic supporting substrate of the same size.

The working mechanism of the FTENG can be explained by the contact-electrification and electrostatic-induction process (Figure 4a). When the PDMS contacts the PTFE film, the electron on the PDMS surface will transfer to the surface of PTFE (I). Once the PDMS leaves, a negative charge will be induced on the carbon fiber; meanwhile, a positive charge will be induced on the copper film (II); then electrons will flow from the copper electrode to the carbon fiber through the external load and finally reach equilibrium (III). This process contributes a positive pulse current output. As the PDMS approaches the PTFE, both the induced negative charges on the carbon fiber and the induced positive charges on the copper film will be reduced, and then electrons will flow from the carbon fiber to the copper (IV) and ultimately reach a new equilibrium, until the PDMS contacts PTFE again (I). This process leads to a negative pulse current output.

The performance of the FTENG driven by a shaker motor was characterized by the open-circuit voltage (V_{OC}) (Figure 4b) and short-circuit current (I_{SC}) (Figure 4c). When the FTENG

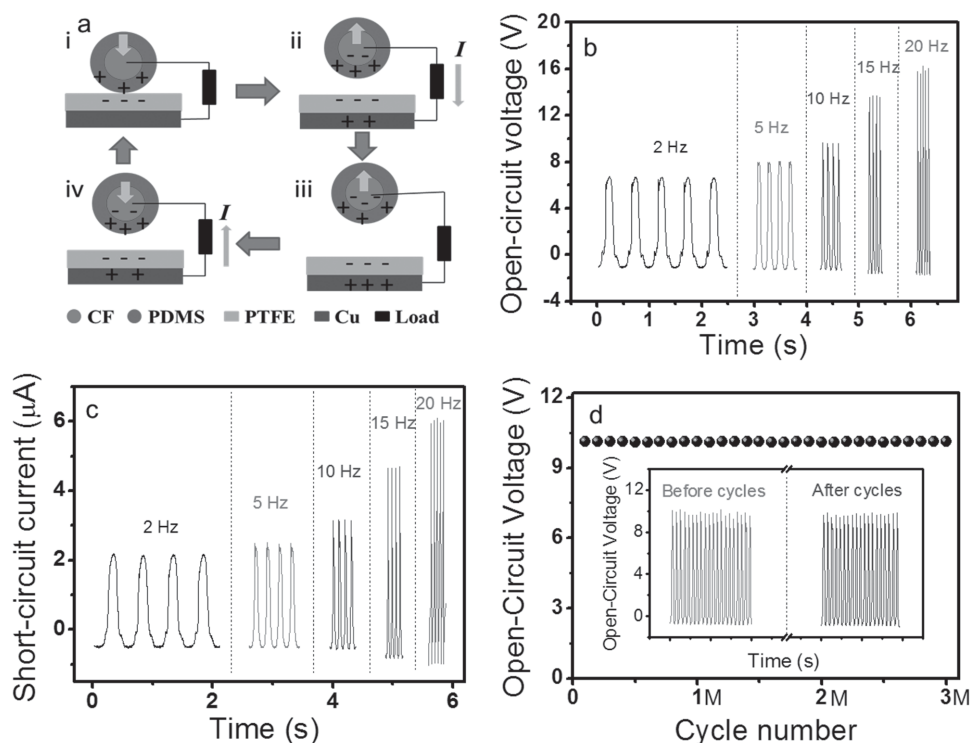


Figure 4. Work mechanism and output performance of FTENG. a) Basic working principle of FTENG, b) open-circuit voltage of FTENG at various frequencies, c) short-circuit current output of FTENG at various frequencies, and d) the stability of the FTENG, inset shows the open-circuit voltage of FTENG before and after 3 000 000 cycles at 10 Hz.

was periodically contacted under a frequency of 2 Hz, a V_{OC} of ≈ 6.7 V was generated between the two electrodes of the FTENG. The V_{OC} increased with the contacting frequency, up to 18 V at 20 Hz. Theoretically, the V_{OC} of the TENG should be constant under various frequencies.^[33] However, the shaker we used also increases the stroke distance of two triboelectric electrodes while increasing frequency, which increases the V_{OC} of the TENG. The periodical contact of FTENG produced a pair of AC short-circuit current peaks in each cycle. The current peak with a larger magnitude of ≈ 2.1 μA came from the pressing motion under a frequency of 2 Hz. The peak value also increased with the contacting frequency, reaching 7 μA at 20 Hz. The output V_{OC} and I_{SC} of the FTENG are smaller than those of some TENGs reported,^[34–36] because the contact area of our wire electrode is far smaller than that of a general TENG. In fact, our output can be boosted simply via increasing the number of parallel workings owing to such tiny diameter (only 0.25 cm). After all, the flexibility of an energy generator is the primary property desired in wearable electronics. To demonstrate the stability of the FTENG, its open-circuit voltage output was tested at 10 Hz for 3 000 000 cycles and it remained nearly 100%, as shown in Figure 4d, indicating a significant stability.

The three-series FSC was charged by the rectified output of FTENG driven by a shake motor, whose electrical circuit diagram is shown in Figure 5a. The charging curve was presented in Figure 5b and Figure S6 (Supporting Information). When the switch S1 is on and switch S2 is off in Figure 5a, the voltage of the FSC linearly increased, indicating the stable output of

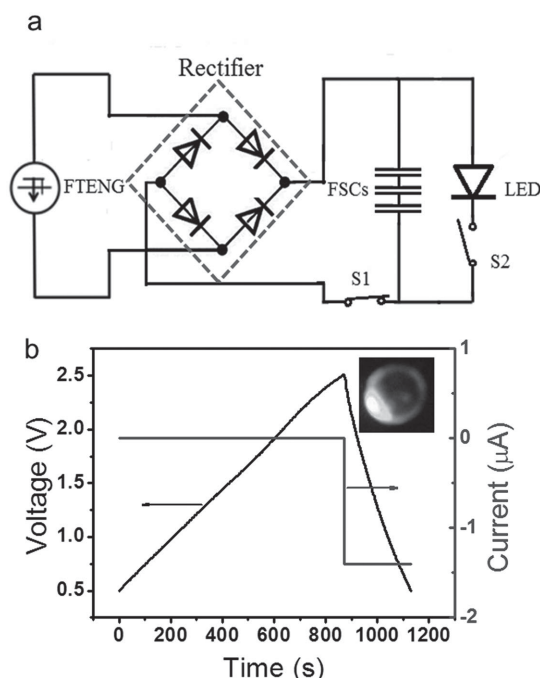


Figure 5. Performance of the FSC-FTENG power system. a) Circuit diagram of the power system and load and b) charging/discharging curves of our FSC charged by the FTENG and discharged at the current load of 1.4 μA , with the inset on the up-right corner showing the lighted LED driven by the FSC as another discharging form.

FTENG and very low leak current of the FSC. It takes only 873 s to charge the FSC from 0.5 to 2.5 V, then 258 s to discharge at a current of 1.4 μA . A green LED (minimum working voltage 2 V) can be lit as an alternate discharging processing, as shown on the upright corner of Figure 5b.

To demonstrate the application of the FTENG and FSC in wearable electronics, we weaved the FTENG and FSC of 1.6 mF on a coat (Figure S7, Supporting Information) to harvest the motion energy while we were jogging. The voltage of the FSC increased by 8 mV during ≈ 10 s, indicating an average charging current of 1.28 μA , when it was charged by the rectified output of FTENG (Figure S7 and Video S1, Supporting Information), which demonstrates that the designed flexible self-charging power system can effectively convert the motion to electricity. The FTENG and FSC can be further weaved into coats and potentially drive the wearable electronics.

In summary, we report a novel flexible self-charging power system that was composed of FSCs and FTENG. The FSC exhibits high capacitance due to the excellent pseudocapacitance of $\text{RuO}_2 \cdot 0.4\text{H}_2\text{O}$ synthesized by the vapor-phase hydrothermal method, which enables it to act as an effective and flexible electronic energy storage device. The weavable FTENG was designed to harvest mechanical energy from human motion. It is demonstrated that the designed self-charging power system is a very competent solution to satisfy the increasing demands of flexible power sources in wearable electronics.

Experimental Section

Synthesis of $\text{RuO}_2 \cdot x\text{H}_2\text{O}@\text{CF}$: The carbon fibers were ultrasonically cleaned in acetone, ethanol, and deionized water for 10 min, respectively, and then coated with RuCl_3 slurry made from 0.05 g of RuCl_3 and 2 mL of ethanol. After the carbon fibers were dried at 60 $^\circ\text{C}$, they were placed on a support and placed in a 50 mL Teflon-lined stainless-steel autoclave with 2 mL of 0.1 M NaOH solution. After sealing, the autoclave was kept in an oven at 190 $^\circ\text{C}$ for 5 h, and then cooled down in air. After washing with deionized water and then drying at 60 $^\circ\text{C}$, $\text{RuO}_2 \cdot x\text{H}_2\text{O}@\text{CF}$ electrodes were obtained.

Fabrication of FSC: The PVA/ H_3PO_4 gel electrolyte was prepared as follows: 5 g of H_3PO_4 was added into 50 mL of deionized water, and then 5 g of poly(vinyl alcohol) (PVA) powder. The mixture was heated to 85 $^\circ\text{C}$ under stirring until the solution became clear. The prepared $\text{RuO}_2 \cdot x\text{H}_2\text{O}@\text{CF}$ electrodes were immersed into PVA/ H_3PO_4 solution for 10 min, with their two-end parts kept above the solution. After being taken out, every two electrodes were assembled onto a PTFE film substrate, leaving aside the bare part as the electrode terminal. When the PVA/ H_3PO_4 gel solidified at room temperature, the flexible FSC was obtained.

Fabrication of FTENG: The carbon fibers were packaged in a tube mold with an inner diameter of 2.5 mm by PDMS. The elastomer and the cross-linker of PDMS were mixed in a 10:1 weight ratio. After the mixture was degassed for 1 h, the carbon fibers were immersed in the mixture and degassed again to fully fill the tube. Heating the mixture further at 80 $^\circ\text{C}$ for 1 h, carbon fibers coated by PDMS were finally obtained by being peeled from the tube mold and then they served as a triboelectric electrode. Another electrode was obtained by sputtering a thin film of Cu (100 nm) on a flexible PTFE film.

Characterization: A Hitachi SU8010 field emission SEM was used to measure the morphology and size of the carbon fiber electrodes. EDS was obtained using an Energy Dispersive Analysis System of X-ray (Oxford INCA). A PANalytical X'Pert PRO diffractometer (Almelo, Netherlands) with $\text{Cu K}\alpha$ radiation ($\lambda = 0.15418$ nm) was employed to measure the XRD patterns of the as-prepared $\text{RuO}_2 \cdot x\text{H}_2\text{O}$. A potentiostat

(Princeton Application Research) was utilized to test the capacitance properties by using CV, GCD, and EIS techniques. For the electric output measurement of the TENG, a shaker motor (Labworks SC121) was applied to drive the TENG contact and separate, a programmable electrometer (Keithley, model 6514), and a low-noise current preamplifier (Stanford Research System, model SR570) were adopted to test the open-circuit voltage and short-circuit current, respectively. The charging/discharging process of the self-charging power system was tested by a battery analyzer (8 channels, MTI).

Supporting Information

Supporting Information is available from the Wiley Online Library or from the author.

Acknowledgements

J.W. and X.L. contributed equally to this work. This research was supported by the Hightower Chair Foundation, the National Science Foundation (DMR-1505319), the "Thousands Talents" program for a pioneer researcher and his innovation team, National Natural Science Foundation of China (21274115), and the program for new century excellent talents at the University of China (Grant No. NCET-11-0433).

Received: April 22, 2015

Revised: May 23, 2015

Published online:

- [1] P. Simon, Y. Gogotsi, *Nat. Mater.* **2008**, *7*, 845.
- [2] Z. L. Wang, J. H. Song, *Science* **2006**, *312*, 242.
- [3] P. X. Gao, J. Song, J. Liu, Z. L. Wang, *Adv. Mater.* **2007**, *19*, 67.
- [4] Q. Wang, X. Wang, J. Xu, X. Ouyang, X. Hou, D. Chen, R. Wang, G. Shen, *Nano Energy* **2014**, *8*, 44.
- [5] S. Wang, Y. Xie, S. Niu, L. Lin, Z. L. Wang, *Adv. Mater.* **2014**, *26*, 2818.
- [6] C. Zhang, W. Tang, C. Han, F. Fan, Z. L. Wang, *Adv. Mater.* **2014**, *26*, 3580.
- [7] Z. L. Wang, *ACS Nano* **2013**, *7*, 9533.
- [8] J. Bae, J. Lee, S. Kim, J. Ha, B.-S. Lee, Y. Park, C. Choong, J.-B. Kim, Z. L. Wang, H.-Y. Kim, J.-J. Park, U. I. Chung, *Nat. Commun.* **2014**, *5*, 4929.
- [9] J. Chen, G. Zhu, W. Yang, Q. Jing, P. Bai, Y. Yang, T.-C. Hou, Z. L. Wang, *Adv. Mater.* **2013**, *25*, 6094.
- [10] Y. Zi, L. Lin, J. Wang, S. Wang, J. Chen, X. Fan, P.-K. Yang, F. Yi, Z. L. Wang, *Adv. Mater.* **2015**, *27*, 2340.
- [11] J. Chen, J. Yang, Z. Li, X. Fan, Y. Zi, Q. Jing, H. Guo, Z. Wen, K. C. Pradel, S. Niu, Z. L. Wang, *ACS Nano* **2015**, *9*, 3324.
- [12] S. Wang, Z.-H. Lin, S. Niu, L. Lin, Y. Xie, K. C. Pradel, Z. L. Wang, *ACS Nano* **2013**, *7*, 11263.
- [13] A. S. Arico, P. Bruce, B. Scrosati, J. M. Tarascon, W. Van Schalkwijk, *Nat. Mater.* **2005**, *4*, 366.
- [14] P. Simon, Y. Gogotsi, B. Dunn, *Science* **2014**, *343*, 1210.
- [15] X. Yang, C. Cheng, Y. Wang, L. Qiu, D. Li, *Science* **2013**, *341*, 534.
- [16] H. Tao, W. Zhu, Y. Fang, Z. Sun, X. Li, *Nanosci. Nanotechnol. Lett.* **2014**, *6*, 497.
- [17] L. Yuan, X.-H. Lu, X. Xiao, T. Zhai, J. Dai, F. Zhang, B. Hu, X. Wang, L. Gong, J. Chen, C. Hu, Y. Tong, J. Zhou, Z. L. Wang, *ACS Nano* **2012**, *6*, 656.
- [18] Z. L. Wang, *Nano Today* **2010**, *5*, 512.
- [19] J. Bae, M. K. Song, Y. J. Park, J. M. Kim, M. Liu, Z. L. Wang, *Angew. Chem. Int. Ed.* **2011**, *50*, 1683.

- [20] J. Ren, L. Li, C. Chen, X. Chen, Z. Cai, L. Qiu, Y. Wang, X. Zhu, H. Peng, *Adv. Mater.* **2013**, *25*, 1155.
- [21] Z. Zhang, X. Chen, P. Chen, G. Guan, L. Qiu, H. Lin, Z. Yang, W. Bai, Y. Luo, H. Peng, *Adv. Mater.* **2014**, *26*, 466.
- [22] Y. Hu, H. Cheng, F. Zhao, N. Chen, L. Jiang, Z. Feng, L. Qu, *Nanoscale* **2014**, *6*, 6448.
- [23] P. Xu, T. Gu, Z. Cao, B. Wei, J. Yu, F. Li, J.-H. Byun, W. Lu, Q. Li, T.-W. Chou, *Adv. Energy Mater.* **2014**, *4*, 1300759.
- [24] B. Liu, B. Liu, X. Wang, D. Chen, Z. Fan, G. Shen, *Nano Energy* **2014**, *10*, 99.
- [25] C.-C. Hu, M.-J. Liu, K.-H. Chang, *J. Power Sources* **2007**, *163*, 1126.
- [26] D. A. McKeown, P. L. Hagens, L. P. L. Carette, A. E. Russell, K. E. Swider, D. R. Rolison, *J. Phys. Chem. B* **1999**, *103*, 4825.
- [27] N. Yoshida, Y. Yamada, S.-I. Nishimura, Y. Oba, M. Ohnuma, A. Yamada, *J. Phys. Chem. C* **2013**, *117*, 12003.
- [28] W. Dmowski, T. Egami, K. E. Swider-Lyons, C. T. Love, D. R. Rolison, *J. Phys. Chem. B* **2002**, *106*, 12677.
- [29] M. Hughes, M. S. P. Shaffer, A. C. Renouf, C. Singh, G. Z. Chen, J. Fray, A. H. Windle, *Adv. Mater.* **2002**, *14*, 382.
- [30] K. Gopalsamy, Z. Xu, B. Zheng, T. Huang, L. Kou, X. Zhao, C. Gao, *Nanoscale* **2014**, *6*, 8595.
- [31] R. Hass, J. Garcia-Canadas, G. Garcia-Belmonte, *J. Electroanal. Chem.* **2005**, *577*, 99.
- [32] W. Guo, X. Zhang, R. Yu, M. Que, Z. Zhang, Z. Wang, Q. Hua, C. Wang, Z. L. Wang, C. Pan, *Adv. Energy Mater.* **2015**, DOI: 10.1002/aenm.201500141.
- [33] S. Niu, Y. S. Zhou, S. Wang, Y. Liu, L. Lin, Y. Bando, Z. L. Wang, *Nano Energy* **2014**, *8*, 150.
- [34] G. Zhu, J. Chen, T. Zhang, Q. Jing, Z. L. Wang, *Nat. Commun.* **2014**, *5*, 3426.
- [35] G. Zhu, Z. H. Lin, Q. Jing, P. Bai, C. Pan, Y. Yang, Y. Zhou, Z. L. Wang, *Nano Lett.* **2013**, *13*, 847.
- [36] G. Cheng, Z.-H. Lin, L. Lin, Z.-L. Du, Z. L. Wang, *ACS Nano* **2013**, *7*, 7383.